LASER & PHOTONICS REVIEWS

www.lpr-journal.org

Nonmagnetic Spoof Plasmonic Isolator Based on Parametric Amplification

Xinxin Gao, Jingjing Zhang, Qian Ma, Wen Yi Cui, Yi Ren, Yu Luo,* and Tie Jun Cui**

Driven by the miniaturization of integrated electronics, research on spoof plasmonic circuits has recently aroused widespread interest. On the other hand, nonreciprocal devices, such as isolators and circulators, are key components of integrated electronic systems. However, bulky magnets required to realize isolation and circulation prevent the application of traditional nonreciprocal technologies to integrated systems. Here, parametric amplification is explored to achieve magnetic-free plasmonic isolation, and an ultrathin reconfigurable spoof plasmonic isolator is realized experimentally. In this isolation system, the forward signal amplified by a spoof plasmonic parametric amplifier is coupled to a second linear plasmonic waveguide via a spoof localized surface plasmon resonator, whereas the transmission from the inverse direction is prohibited, giving rise to a measured isolation ratio of up to 20 dB. By tuning the nonlinear phase-matching condition through external bias voltage, multifrequency isolation of spoof surface plasmon polariton (SSPP) signals is also realized experimentally. This work demonstrates the possibility of producing miniaturized and low-cost nonreciprocal SSPP devices, holding great promise for applications in nonmagnetic information processing and radar detection.

1. Introduction

High-speed and reliable information transfer with high signal integration is highly desired for future on-chip communication.[1] Spoof surface plasmon polaritons (SSPPs) provide a possible route to achieve this goal. SSPPs, first proposed by Pendry and coworkers in 2004,[2] are surface electromagnetic waves propagating along the metal surface with subwavelength corrugations at microwave and terahertz frequencies, mimicking the characteristic of optical surface plasmon polaritons.[3,4] To facilitate their practical applications, especially to integrated circuits, spoof plasmonic metamaterials have undergone a change from three-dimensional bulk structures to conformal ultrathin corrugated metallic strips.[5] Compared to the conventional microstrip line widely used by the microwave community, the ultrathin SSPP waveguide has several distinct advantages such as low loss and compact size due to the tight field-confinement feature.[6,7,42,43] More importantly, the SSPP waveguides can be packed in a highly dense manner in a circuit, where the crosstalk between parallel waveguides is effectively suppressed.[8–10,37] Motivated by these merits, many circuit elements have been fabricated and implemented experimentally in the spoof plasmonic platform.[11–15] However, most SSPP devices realized thus far are passive and reciprocal. In integrated electronic circuits, nonreciprocity is highly desired to reach asymmetric signal transmission and modulation, and nonreciprocal microwave components, such as isolators, circulators, and gyrators, play a critical role in modern communication, radar, and sensing systems.[16]

Based on the Lorentz reciprocity theorem, any linear and time-invariant media with symmetric permittivity and permeability tensors are inherently reciprocal. To break the time-reversal symmetry, magnetic biasing from ferrite materials has been widely deployed.[17–19] Various ferrite-magnetic nonreciprocal devices were proposed and even commercialized. However, due to the inevitable permanent magnet required to bias the ferrite, these devices are bulky in size, expensive to fabricate, and incompatible with the integrated circuit technologies.[16] Such drawbacks associated with magneto-optics have motivated researchers to explore different schemes to achieve magnetic-free nonreciprocity. One straightforward way readily available in the semiconductor integrated circuits relies on the intrinsic nonreciprocal nature of active transistors, where unidirectional gain can be exhibited by applying a biased DC voltage or current on the transistors.[20–23] Although these devices have merits of high integration and low cost, the poor noise performance and low power capacity have limited their applications.[24] Spatiotemporal modulations, which rely on time variations of permittivity or conductivity to break the reciprocity, are arguably a promising scheme

X. Gao, J. Zhang, Q. Ma, W. Y. Cui, Y. Ren, T. J. Cui
Institute of Electromagnetic Space
Southeast University
Nanjing 210096, China
E-mail: zhangjingjing@seu.edu.cn; tjcui@seu.edu.cn

X. Gao, J. Zhang, Q. Ma, W. Y. Cui, Y. Ren, T. J. Cui
State Key Laboratory of Millimeter Waves
Southeast University
Nanjing 210096, China

Y. Luo
School of Electrical and Electronic Engineering
Nanyang Technological University
Nanyang Avenue 639798, Singapore
E-mail: luoyu@ntu.edu.sg

The ORCID identification number(s) for the author(s) of this article can be found under https://doi.org/10.1002/lpor.202100578

DOI: 10.1002/lpor.202100578

to tackle these challenges.[25–28,38,39] However, the reductions of device size and modulation-circuit complexity compromise the performance (e.g., bandwidth and modulation depth), and the enhancement of performance still demands further research. Another alternative approach to achieve the nonreciprocal response is breaking the linearity. For example, the nonreciprocal transmissions can be realized via asymmetric structures loaded with materials with the second-order or Kerr susceptibility.[29–33] Such nonreciprocal transmissions have the advantages of low power consumption and easy integration. However, theoretical works show that the nonlinear-based isolators cannot suppress unknown backward noise owing to the dynamic reciprocity of the nonlinear susceptibility.[34] Whether the nonlinear devices can provide good isolation performance or not remains a controversial question.

Here, we propose and experimentally demonstrate the first magnetic-free SSPP isolator, which is achieved by exploiting a phase-matched spoof plasmonic parametric amplifier in three-wave mixing. In this amplifier, the nonlinearity of a semiconductor diode is exploited to impart gain to the desired signal with a pump signal, accompanied by an idler signal whose frequency is equal to the difference between pump and input frequencies. The amplified signals are then selected and coupled to a linear SSPP waveguide through the near-field coupling with a spoof localized surface plasmon resonator. Our proposed SSPP isolator not only inherits the advantages of conformal SSPPs including compactness, integration, and low cost but also has remarkable isolating performance in suppressing the transmission of backward-propagating noise. Furthermore, multifrequency isolation is enabled by manipulating the dispersion behaviors of the active SSPP structures. Our scheme opens a door toward the plasmonic-based magnetic-free nonreciprocity for potential applications in communications, radar, and integrated circuits.

2. Design and Experimental Results

The proposed isolator consists of a spoof plasmonic parametric amplifier (PA), two spoof localized surface plasmon (SLSP) resonators, and a spoof surface plasmon polariton (SSPP) waveguide, as shown in **Figure 1**a. The SLSP structure is designed to resonate at the same frequency as that of the signal wave so that the forward signal wave from port 1 propagating along the spoof plasmonic PA can be coupled to the SLSP resonator. When the upper and lower SSPP waveguides have the same phase constants at the signal frequency, this corresponding power flow at the excitation resonance frequency of SLSPs will be transmitted counter-clockwise to port 3 of the passive SSPP waveguide.[35] For forward input signal wave, the corresponding signal gain can be obtained under the phase-matching condition, indicating the momentum conservation ($k_p = k_s + k_i$, where k_p, k_s, and k_i are the wavenumbers of the pump, signal, and idler, respectively) and the energy conservation ($f_p = f_s + f_i$, where f_p, f_s, and f_i are the frequencies of the pump, signal, and idler, respectively). In the case of the same pump wave input, the backward signal wave cannot be amplified due to phase-mismatching. Thus, the Lorentz reciprocity is broken in this nonlinear spoof plasmonic device. Additionally, we can fabricate the upper and lower SSPP waveguides with different cutoff frequencies. Compared to the isolator with two identical waveguides, the proposed device does not need to introduce an additional filter to suppress excessive pump waves.[36] More importantly, due to the flexibility of dispersion behaviors of the SSPP waveguide loaded with the varactor, a reconfigurable nonreciprocal transmission can be realized via tuning the bias voltage applied to spoof plasmonic PA.

The occurrence of efficient nonreciprocal transmission in the presented device requires that two fundamental conditions are satisfied simultaneously for the proposed isolator: 1) the signal frequency overlaps the localized spoof plasmonic resonance frequency; 2) the phase constants of the active and passive SSPP waveguides at the signal frequency should be the same so that the optical momentum is preserved. These requirements can be realized by properly designing different unit structures. Note that the signal frequency of spoof plasmonic PA needs to meet the phase-matching condition. The corresponding unit structure is designed as shown in Figure 1b, and the structural parameters are $s = 0.250$ mm, $a = 1.250$ mm, $a_1 = 0.500$ mm, $a_2 = 0.400$ mm, $d = 1.000$ mm, $d_0 = 1.500$ mm, $d_1 = 1.000$ mm, $d_2 = 3.250$ mm, and $p = 2.500$ mm. Meanwhile, the varactor is loaded between the upper and lower branches of the spoof plasmonic unit structure, introducing nonlinearity and adjustability. Moreover, to obtain a resonance frequency close to the signal frequency and further enhance the SSPP-SLSP coupling, two SLSP resonators with an interval of $s_0 = 0.140$ mm are fabricated, as illustrated in Figure 1c, where $R = 8.680$ mm and $r = 2.000$ mm. Finally, to achieve the identical phase constants of the active and passive SSPP waveguides, the unit structure of the passive SSPP waveguide is shown in Figure 1d, where $a_3 = 0.500$ mm, $h = 5.300$ mm, $p = 2.500$ mm, and $w = 0.500$ mm. These unit structures are fabricated on a dielectric substrate of Rogers 5880 with a thickness of 0.787 mm, a relative dielectric constant of 2.2, and tangent loss of 0.0009.

We investigate the phase constant of signal wave and the resonance frequency of SLSP structure via the dispersion behaviors of the SSPP waveguides and the extinction cross-section (ECS) spectra of the SLSP resonator (see Section 4.1). The dispersion curves of the SSPP structure in panel (b) are sketched in Figure 1e, where the wave vectors of pump, signal, and idler SSPP waves satisfy $k_p = k_s + k_i$ and $f_p = f_s + f_i$. When the capacitance loaded on the spoof plasmonic unit structure is 0.18 pF, the signal frequency and the corresponding phase constant are 6.034 GHz and 377.00 m^{-1}, respectively. Furthermore, owing to the loss of the SSPP structure, the attenuation constant of the signal wave is 5.32 m^{-1}. The ECS spectra of SLSP structures versus the frequency are illustrated in Figure 1f, where a peak at the resonance frequency of 6.036 GHz can be observed, corresponding to a quadrupole resonance mode (see the near-field distribution in the inset). This resonance frequency is close to the signal frequency of spoof plasmonic PA. Additionally, the dispersion behaviors of the passive SSPP unit structure are studied as shown in Figure 1g. We observe that the phase constant at 6.034 GHz in the passive waveguide is about 321.00 m^{-1}, which approximately equals that of the parametric amplification signal. Therefore, the two conditions mentioned above are satisfied.

More importantly, when the capacitance loaded on the spoof plasmonic unit structure is switched to 0.17 and 0.19 pF, different phase-matching points can be obtained, as shown in Figure S1a,b (Supporting Information). When the pump frequency remains constant, changing the capacitance of the loaded varactor gives rise to the variation of dispersion behaviors, allowing different

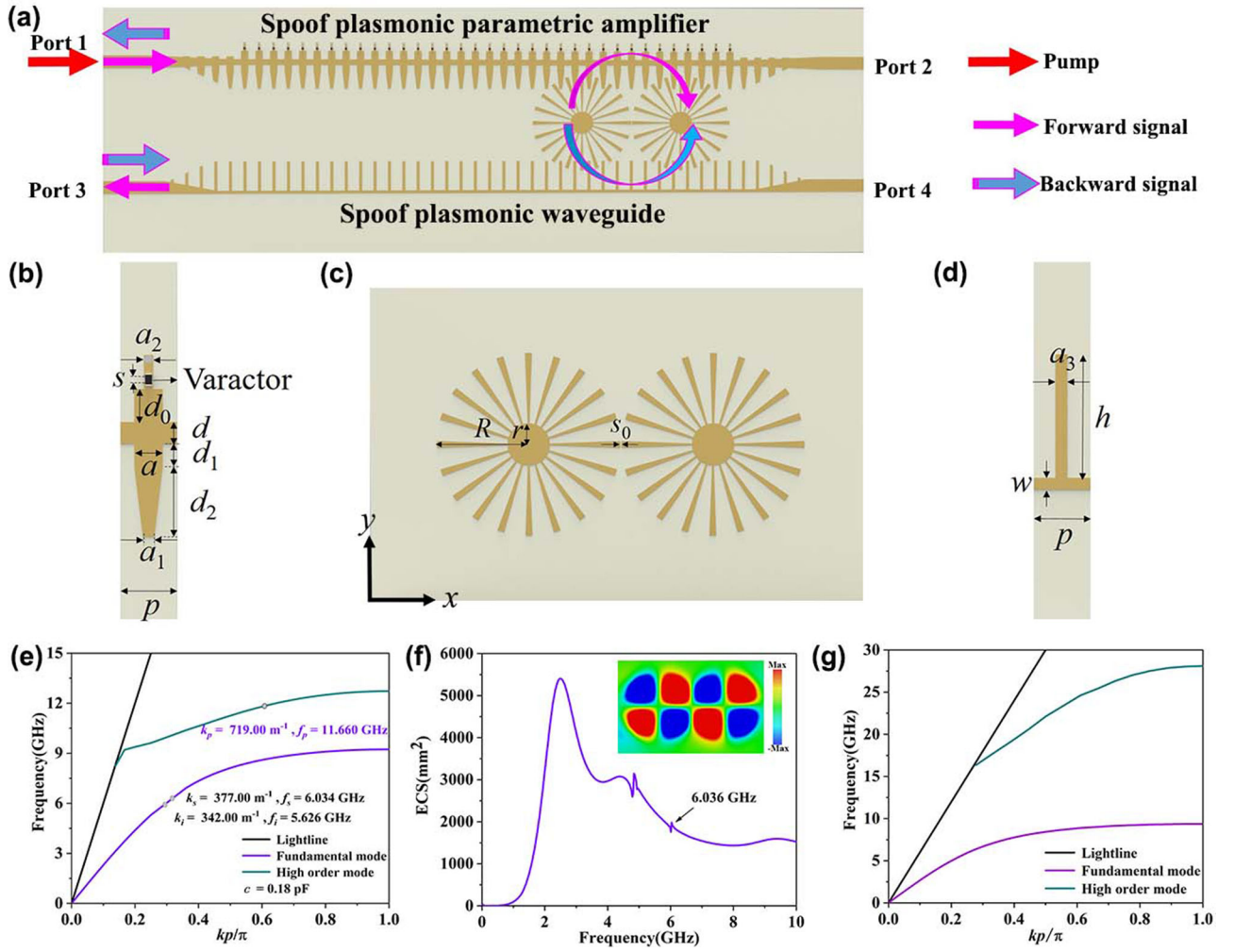

Figure 1. a) Schematic of forward and backward propagation configurations based on signal inputs at ports 1 and 3. b) Unit structure of spoof SPP parametric amplifier loaded with the varactor diode, where $s = 0.250$ mm, $a = 1.250$ mm, $a_1 = 0.500$ mm, $a_2 = 0.400$ mm, $d = 1.000$ mm, $d_0 = 1.50$ mm, $d_1 = 1$ mm, $d_2 = 3.250$ mm, and $p = 2.500$ mm. c) LSP structure, where $R = 8.680$ mm, $r = 2.000$ mm, and $s_0 = 0.140$ mm. d) Passive spoof SPP unit structure, where $a_3 = 0.500$ mm, $h = 5.300$ mm, $p = 2.500$ mm, and $w = 0.500$ mm. e) The simulated dispersion behaviors of spoof SPP parametric amplification with the capacitance $c = 0.18$ pF. The condition for phase matching is $k_p = 719.00$ m^{-1} at $f_p = 11.660$ GHz, $k_s = 377.00$ m^{-1} at $f_s = 6.034$ GHz, and $k_i = 342.00$ m^{-1} at $f_i = 5.626$ GHz. Note that owing to the loss of varactor diode their attenuous constants are 13.40, 5.32, and 3.95 m^{-1}. f) The simulated ECS of SLSP resonators and the near-field distributions at the resonance frequency of 6.036 GHz. g) The dispersion relation of passive SSPP, where the phase constant at 6.034 GHz is 321.00 m^{-1}.

phase-matching conditions to be satisfied on the same device. Therefore, based on parametric amplification of the SSPP signal at multiple frequencies, a reconfigurable isolator can be realized. Note that the working frequencies of the isolator are restricted by the narrow resonance band of the SLSP structure.

For the proposed isolator based on parametric amplification, the isolation ratio mainly depends on the amplified signal gain. To achieve a large isolation ratio, high signal gain generated from the designed PA is necessary. Based on the theoretical model for spoof plasmonic parametric amplification,[11] we can predict that the maximum signal gain can be realized at the nonlinear length of about 5λ (λ is the signal wavelength of SSPP). Thus, we fabricate the spoof plasmonic PA consisting of 35-unit cells loaded with the varactors (MAVR-011020-1141), corresponding to the nonlinear length of 87.500 mm. According to the comparison between simulated and measured transmission parameters, we can estimate the capacitance and the bias voltage of the varactors, as shown in Figure S1c–e (Supporting Information). When the bias voltages applied to the varactor are 1.25, 1.11, and 1.02 V, the corresponding capacitances are 0.17, 0.18, and 0.19 pF, respectively. Moreover, the simulated transmission parameters of the passive SSPP waveguide are shown in Figure S1f (Supporting Information).

We start from the case with a bias voltage of 1.11 V (corresponding to the capacitance of 0.18 pF) to observe the transmission property of the proposed device without applying the pump wave. Transmission dip around 6.034 GHz is observed due to the coupling between SSPPs and SLSPs (**Figure 2**a). Most of the signal energy at this narrow frequency band is then coupled to the passive SSPP waveguide, yielding a transmission peak

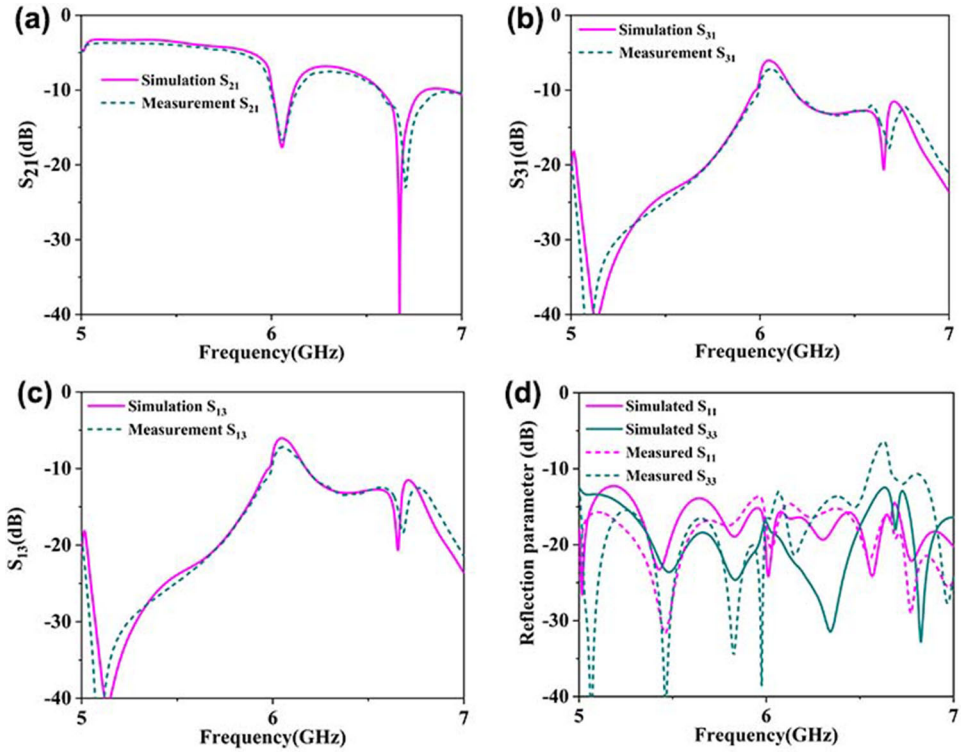

Figure 2. Simulated and measured linear transmission parameters of the spoof plasmonic isolator based on parametric amplification, where the reciprocal transmission is obtained. a) The transmission parameters from port 1 to 2 (S_{21}). b) The transmission parameters from port 1 to 3 (S_{31}). c) The transmission parameter from port 3 to 1 (S_{13}). d) The reflection parameters S_{11} and S_{33}. The simulated and measured linear transmission results are obtained when the corresponding capacitance and the bias voltage are 0.18 pF and 1.11 V, respectively.

of S_{31}, as shown in Figure 2b. As illustrated in Figure 2c, owing to the Lorentz reciprocity, transmission parameters between ports 1 and 3 are consistent (S_{31} is equal to S_{13}). It is worth noting that this proposed device has almost no scattering at ports 1 and 3 (Figure 2d), maintaining the desired directionality of the momentum conservation. We can also clearly observe that the measured results agree remarkably well with the simulated results. As a result, the incident signal wave from spoof plasmonic PA can be efficiently coupled into the passive SSPP waveguide via the SLSP resonances, serving as a good basis to achieve high isolation.

A comprehensive set of measurements has been carried out to experimentally confirm the nonreciprocal transmission of the proposed isolator with spoof plasmonic PA, as illustrated in **Figure 3**a (see Section 4.2). Here, the transmission performance of forward and backward signal waves can be represented by transmission parameters from port 1 to port 3 (S_{31}) and transmission parameters from port 3 to port 1 (S_{13}), respectively. Theoretical analysis indicates that when the pump intensity reaches a certain constant, the signal wave will be amplified.[11] As expected, the reciprocal transmissions of the forward and backward signal waves are verified by turning the pump off, as shown in Figure 3b. When the pump wave is switched to an on state, the amplification of the forward signal can be observed, provided that the signal gain compensates for the losses of structure and varactors. Note that the transmission peak occurs at the pump frequency of 11.680 GHz and the signal frequency of 6.034 GHz, indicating that the phase-matching condition of parametric amplification is satisfied when the applied bias voltage is set as 1.11 V. The power of the forward signal output from the port 3 is much higher than that of the backward signal, demonstrating the typical nonreciprocal transmission property.

Additionally, due to the flexibility in tuning SSPP dispersion behaviors, the isolation at multiple frequencies can also be realized with different bias voltages. As sketched in Figure 3c, when the applied bias voltage is switched to 1.02 V, the transmission peak of the forward signal wave occurs at 6.000 GHz. In addition, when this bias voltage is 1.25 V, the transmission of the forward signal wave reaches its maximum at 6.086 GHz, as shown in Figure 3d. Here, the pump frequency and intensity remain unchanged at 11.680 GHz and 24 dBm, respectively. Note that due to the device loss, the transmission peaks under different forward signal waves have different amplitudes. Thus, the isolation at different phase-matching frequency points is different. Furthermore, in order to observe the nonreciprocity phenomenon more intuitively, the near-field distribution under forward/backward wave at 6.034 GHz is measured via the near-field measurement setup (details in Section S2, Supporting Information), as shown in Figure 3e,f. Nonreciprocal transmission can be intuitively observed, where the forward signal from port 1 returns more energy into port 3 than the backward signal from port 3 to port 1 with the pump wave turned on. In contrast, the near field distribution with pump-off shown in Figure S3 demonstrates the reciprocal characteristic.

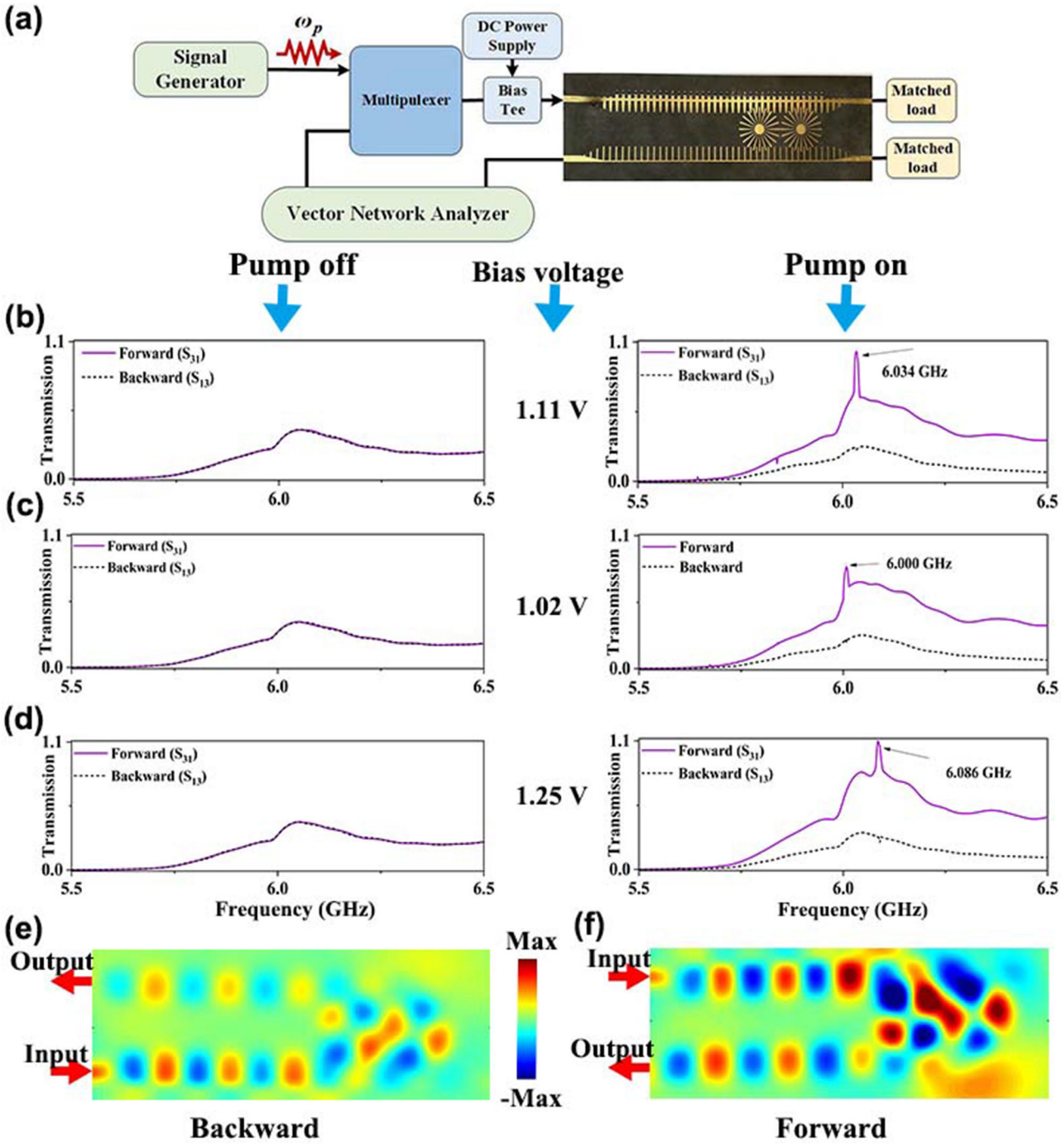

Figure 3. Isolation at different bias voltages. a) Schematic of the experimental setup for isolation measurements on the proposed nonlinear isolator. (b)–(d) show transmission behaviors when the bias voltages applied to the varactor are 1.11, 1.02, and 1.25 V, respectively. The reciprocal transmission is obtained when the pump intensity is off. The typical asymmetric transmission occurs when the parametric gain obtained by the spoof SPP parametric amplifier compensates for the loss. The pump intensity and frequency are 24 dBm and 11.680 GHz, and the signal power is −5 dBm. (e) and (f) show the measured near-field distributions of the backward and forward signal waves at 6.034 GHz, respectively, where the bias voltage is 1.11 V and the incident pump intensity is 24 dBm.

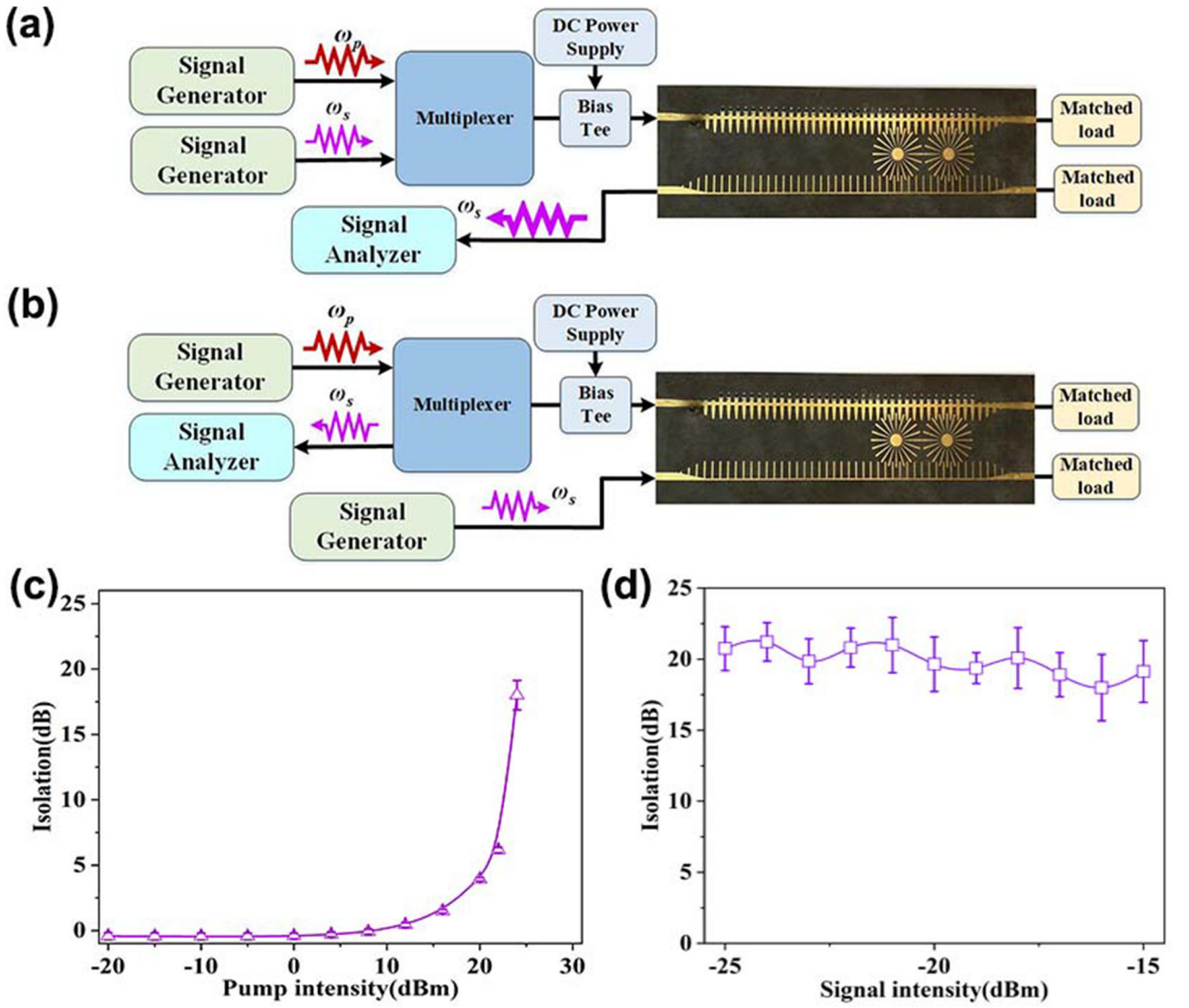

Figure 4. Isolation versus varied pump intensity and signal intensity. (a) and (b) depict the experimental setups employed to measure the isolation ratio under the phase-matching and the phase-mismatching conditions, respectively. c) The isolation versus the pump intensity from −25 to 23 dBm at the constant of signal intensity (−20 dBm) and signal frequency (6.034 GHz). d) The isolation versus the signal intensity from −25 to −15 dBm at the constant of pump intensity (24 dBm) and pump frequency (11.680 GHz). The error bars in all figures indicate the system uncertainly in the respective measurements and have been calculated by taking the standard deviations of the measured isolation ratio under the same pump intensity and signal intensity.

Figure 4a,b present the measurement setups of the forward and backward signal to collect the isolation ratio as a function of the pump and signal intensities (see Section 4.2), respectively. Here, the applied bias voltage and the pump frequency are 1.11 V and 11.680 GHz, respectively. The dependence of the isolation on the incident pump intensities varying from −20 to 24 dBm is illustrated in Figure 4c. When the incident pump intensity progressively enhances, the isolation ratio rises gradually from 0 to 20 dB. Note that the isolation begins to increase when the pump intensity reaches a certain constant, indicating that the signal gain exceeds the structural loss. Moreover, due to the thermal effect induced by the pump power, the isolation peak frequency shows a blue shift as the pump intensity increases (see Figure S4, Supporting Information). In the above process, the input intensities of forward and backward signal waves are maintained with an equal intensity of −20 dBm. When the pump intensity remains at 24 dBm, the transmission changes with the input signal intensity, as shown in Figure S5 (Supporting Information). For the spoof plasmonic PA, when the forward signal is large enough, the incident pump intensity will exist in the depletion problem. Namely, there is not enough pump intensity to supply the signal wave for amplification. Thus, the peak at 6.034 GHz gradually drops as the signal intensity increases, as shown in Figure S5 (Supporting Information). Meanwhile, the collected isolation ratio versus the signal intensity is shown in Figure 4d. The isolation of the proposed device remains a constant of about 20 dB when the incident signal intensity is from −25 to −15 dBm, indicating that it can suppress backward noise transmission.

3. Conclusion

We have demonstrated experimentally a reconfigurable nonmagnetic isolator with parametric amplification realized on an ultrathin planar spoof plasmonic platform. The SSPP dispersion behaviors can be engineered so that the phase-matching condition of parametric amplification for forward signals can be achieved at multiple frequencies, enabling the multifrequency isolation. Note that due to the high Q-factor of the SLSP resonator for separating the signal wave from the pump and idler waves, the tunability of the isolator is restricted in a very narrow frequency range. As a future step, active elements will be implemented into the SLSP resonators to improve the tunable range, and the operating frequency may be extended to the Terahertz frequency via introducing graphene with high nonlinearity and modulation conductivity[39-41,44] into the SSPP structure. We envision this work could establish a foundation for developing magnetic-free nonreciprocal isolation SSPP devices suitable for on-chip integration with microwave circuits, with the potentials to revolutionize applications in communication and radar systems.

4. Simulation and Experimental Methods

4.1. Simulation Method

Here, the dispersion behaviors of SSPP structures are investigated with Eigen-mode Solver of the Commercial software CST Microwave Studio, where the periodic boundary condition is applied to the propagation direction of the electromagnetic wave, and the electric boundary condition is applied to the other two boundaries in the orthogonal direction. Moreover, we can obtain the ECS and resonance frequency of SLSP structures by the Time Domain Solver, where an incoming plane wave propagating along the *y*-direction with the electric polarized in the *x*-direction is considered.

4.2. Experimental Method

In order to measure transmission parameters and signal isolation of the sample, we built two different test platforms. For the measurement of transmission parameters with different pump intensities, we use the signal generator (Agilent E8267D) and vector network analyzer (Agilent N5230C). The pump wave and signal wave are generated from the signal generator and vector network analyzer, respectively, and integrated into a multiplexer connected with port 1 of the sample. The other port of VNA is connected with port 3 of the sample. To measure the forward scattered power spectra of the designed sample, the pump and signal intensities created from two signal generators (Agilent E8267D and E8257D) are merged using a multiplexer into a single signal to excite the nonlinear SSPP waveguide. The output signal intensities of port 3 are collected by the signal analyzer (Agilent N9010A). For the backward scatted power spectra, the signal generator (Agilent E8267D) and the signal analyzer are connected with a multiplexer and the signal generator (Agilent E8257D) is connected with port 3 of the sample, respectively. Note that a bias Tee is placed between the multiplexer and the sample to feed the RF signal and DC bias into the sample simultaneously. Ports 2 and 4 are loaded with 50 ohm matched load to avoid the sample reflection.

Supporting Information

Supporting Information is available from the Wiley Online Library or from the author.

Acknowledgements

X.G. and J.Z. contributed equally to this work. This work was supported in part from the National Natural Science Foundation of China (61871127, 61735010, 61731010, 61890544, 61801117, 61722106, 61701107, 61701108, and 61701246), National Key Research and Development Program of China (2017YFA0700201, 2017YFA0700202, and 2017YFA0700203), Fundamental Research Funds for the Central Universities (2242018R30001), State Key Laboratory of Millimeter Waves, Southeast University, China (K201924), 111 Project (111-2-05), and Fund for International Cooperation and Exchange of the National Natural Science Foundation of China (61761136007). Y.L. acknowledges funding support from Singapore Ministry of Education (MOE2018-T2-2-189(S)), A*Star AME IRG Grant (A20E5c0095), Programmatic Funds (A18A7b0058), and National Research Foundation Singapore Competitive Research Program (NRF220 CRP22-2019-0006 and NRF-CRP23-2019-0007).

Conflict of Interest

The authors declare no conflict of interest.

Data Availability Statement

The data that support the findings of this study are available from the corresponding author upon reasonable request.

Keywords

nonreciprocal transmission, reconfigurable isolators | spoof plasmonic parametric amplifiers, spoof surface plasmon polaritons

Received: October 10, 2021
Revised: December 22, 2021
Published online:

[1] S. R. Joy, M. Erementchouk, H. Yu, P. Mazumder, *IEEE Trans. Commun.* **2019**, *67*, 599.
[2] J. B. Pendry, L. Martin-Moreno, F. J. Garcia-Vidal, *Science* **2004**, *305*, 847.
[3] S. A. Maier, S. R. Andrew, L. M. Moreno, F. J. Garcia-Vidal, *Phys. Rev. Lett.* **2006**, *97*, 176805.
[4] F. J. Garcia-Vidal, L. Martín-Moreno, J. B. Pendry, *J. Opt. A: Pure Appl. Opt.* **2005**, *7*, S97.
[5] X. Shen, T. J. Cui, D. Martin-Cano, F. J. Garcia-Vidal, *Proc. Natl. Acad. Sci. USA* **2013**, *110*, 40.
[6] J. Zhang, H. C. Zhang, X. Gao, L. P. Zhang, L. Y. Niu, P. H. He, T. J. Cui, *Sci. Bull.* **2019**, *64*, 843.
[7] A. Kianinejad, Z. N. Chen, C.-W. Qiu, *IEEE Trans. Microw. Theory Techn.* **2016**, *64*, 3078.

[8] H. C. Zhang, L. P. Zhang, P. H. He, J. Xu, Q. Xu, F. J. Garcia-Vidal, T. J. Cui, *Light: Sci. Appl.* **2020**, *9*, 113.
[9] H. C. Zhang, T. J. Cui, Q. Zhang, Y. Fan, X. Fu, *ACS Photonics* **2015**, *2*, 1333.
[10] X. Gao, H. C. Zhang, P. H. He, Z. X. Wang, J. Lu, R. T. Yan, T. J. Cui, *IEEE Trans. Compon., Packag., Manuf. Technol.* **2019**, *9*, 2267.
[11] X. Gao, J. Zhang, Y. Luo, Q. Ma, G. D. Bai, H. C. Zhang, T. J. Cui, *Adv. Sci.* **2021**, *8*, 2100795.
[12] H. C. Zhang, T. J. Cui, Y. Luo, J. Zhang, J. Xu, P. H. He, L. P. Zhang, *Nat. Sci. Rev.* **2020**, *7*, 261.
[13] X. Tian, P. M. Lee, Y. J. Tan, T. L. Y. Wu, H. Yao, M. Zhang, Z. Li, K. A. Ng, B. C. K. Tee, J. S. Ho, *Nat. Electron.* **2019**, *2*, 243.
[14] X. Gao, H. C. Zhang, L. W. Wu, Z. X. Wang, P. H. He, Z. Gao, T. J. Cui, *IEEE Trans. Antennas Propag.* **2020**, *68*, 1558.
[15] X. Gao, J. Zhang, H. C. Zhang, L. Liu, Q. Ma, P. Xu, T. J. Cui, *Adv. Opt. Mater.* **2020**, *8*, 1902058.
[16] A. Kord, D. L. Sounas, A. Alù, *Proc. IEEE* **2020**, *108*, 1728.
[17] E. Schlomann, *IRE Trans. Microwave Theory Tech.* **2003**, *8*, 199.
[18] J. D. Adam, L. E. Davis, G. F. Dionne, E. F. Schloemann, S. N. Stitzer, *IEEE Trans. Microwave Theory Tech.* **2002**, *50*, 721.
[19] Y. Konishi, *IEEE Trans. Microwave Theory Tech.* **1965**, *MT13*, 852.
[20] Q. Ma, L. Chen, H. B. Jing, Q. R. Hong, H. Y. Cui, Y. Liu, L. Li, T. J. Cui, *Adv. Opt. Mater.* **2019**, *7*, 1901285.
[21] S. Tanaka, N. Shimomur, K. Ohtake, *Proc. IEEE* **1965**, *53*, 260.
[22] Y. Ayasli, *IEEE Trans. Magn.* **1989**, *25*, 3242.
[23] L. Jongsoo, J. D. Cressler, A. J. Joseph, *IEEE Microwave Wireless Compon. Lett.* **2005**, *15*, 220.
[24] G. Carchon, B. Nauwelaers, *IEEE Trans. Microwave Theory Tech.* **2000**, *48*, 316.
[25] S. Qin, Q. Xu, Y. E. Wang, *IEEE Trans. Microwave Theory Tech.* **2014**, *62*, 2260.
[26] A. Kord, D. L. Sounas, A. Alù, *IEEE Trans. Microwave Theory Tech.* **2018**, *66*, 911.
[27] N. A. Estep, D. L. Sounas, J. Soric, A. Alù, *Nat. Phys.* **2014**, *10*, 923.
[28] Z. Yu, S. Fan, *Nat. Photonics* **2009**, *3*, 91.
[29] D. L. Sounas, J. Soric, A. Alù, *Nat. Electron.* **2018**, *1*, 113.
[30] S. Lepri, G. Casati, *Phys. Rev. Lett.* **2011**, *106*, 164101.
[31] B. Peng, S. K. Ozdemir, F. Lei, F. Monifi, M. Gianfreda, G. L. Long, S. Fan, F. Nori, C. M. Bender, L. Wang, *Nat. Phys.* **2014**, *10*, 394.
[32] L. Chang, X. Jiang, S. Hua, C. Yang, J. Wen, L. Jiang, G. Li, G. Wang, M. Xiao, *Nat. Photonics* **2014**, *8*, 524.
[33] N. Bender, S. Factor, *Phys. Rev. Lett.* **2013**, *110*, 234101.
[34] Y. Shi, Z. Yu, S. Fan, *Nat. Photonics* **2015**, *9*, 388.
[35] H. Su, X. Shen, G. Su, L. Lin, J. Ding, F. Liu, Z. Peng, Y. Liu, Z. Wang, *Laser Photonics Rev.* **2018**, *12*, 201800010.
[36] S. Hua, J. Wen, X. Jiang, Q. Hua, L. Jiang, M. Xiao, *Nat. Commun.* **2016**, *7*, 13657.
[37] X. T. Yan, W. Tang, J. F. Liu, M. Wang, X. X. Gao, T. J. Cui, *Adv. Photonics* **2021**, *3*, 026001.
[38] Y. Hadad, J. C. Soric, A. Alù, *Proc. Natl. Acad. Sci. USA* **2016**, *113*, 3471.
[39] D. C. Serrano, J. S. Gomez-Diaz, D. L. Sounas, Y. Hadad, A. Alvarez-Melcon, A. Alù, *IEEE Antennas Wireless Propag. Lett.* **2015**, *15*, 1529.
[40] I. S. Byun, D. Yoon, J. S. Choi, I. Huang, D. H. Lee, M. J. Lee, T. Kawai, Y. W. Son, Q. Jia, H. Cheong, B. H. Park, *ACS Nano* **2011**, *5*, 6417.
[41] Y. Hadad, B. Z. Steinberg, *Phys. Rev. B* **2013**, *88*, 075439.
[42] Z. Gao, L. Wu, F. Gao, Y. Luo, B. Zhang, *Adv. Mater.* **2018**, *30*, 1706683.
[43] H. Hu, X. Lin, L. J. Wong, Q. Yang, D. Liu, B. Zhang, Y. Luo, *eLight* **2022**, https://doi.org/10.1186/s43593-021-00009-5
[44] T. Wu, Y. Luo, S. A. Maier, L. Wei, *Phys. Rev. Appl.* **2019**, https://doi.org/10.1103/physrevapplied.11.014049